Band Residual Difference Algorithm for Retrieval of SO_2 From the Aura Ozone Monitoring Instrument (OMI)

Nickolay A. Krotkov, Simon A. Carn, Arlin J. Krueger, Pawan K. Bhartia, and Kai Yang

***Abstract*—The Ozone Monitoring Instrument (OMI) on EOS/Aura offers unprecedented spatial and spectral resolution, coupled with global coverage, for space-based UV measurements of sulfur dioxide (SO_2). This paper describes an OMI SO_2 algorithm (the band residual difference) that uses calibrated residuals at SO_2 absorption band centers produced by the NASA operational ozone algorithm (OMTO3). By using optimum wavelengths for retrieval of SO_2, the retrieval sensitivity is improved over NASA predecessor Total Ozone Mapping Spectrometer (TOMS) by factors of 10 to 20, depending on location. The ground footprint of OMI is eight times smaller than TOMS. These factors produce two orders of magnitude improvement in the minimum detectable mass of SO_2. Thus, the diffuse boundaries of volcanic clouds can be imaged better and the clouds can be tracked longer. More significantly, the improved sensitivity now permits daily global measurement of passive volcanic degassing of SO_2 and of heavy anthropogenic SO_2 pollution to provide new information on the relative importance of these sources for climate studies.**

***Index Terms*—Anthropogenic pollution, Aura, Ozone Monitoring Instrument (OMI), SO_2, volcanic degassing.**

I. Introduction

SULFUR dioxide is now recognized as the primary volcanic agent of climate change. SO_2 is converted to a sulfate aerosol that has a long lifetime in the stratosphere. The first quantitative data on the mass of SO_2 in a major eruption (El Chichon, 1982) was obtained from the six-UV band NASA Nimbus-7 Total Ozone Mapping Spectrometer (TOMS) [1]. All significant eruptions since 1978 have now been measured by the series of TOMS instruments [Nimbus-7, Meteor-3, ADEOS I, Earth Probe (EP)] [2]–[7]. The SO_2 detection sensitivity was limited to large volcanic clouds by the discrete TOMS wavelengths that were designed for total ozone measurements [8]. EP TOMS has had limited success in detecting noneruptive degassing from exceptionally strong volcanic sources [9] and large SO_2 pollution events [10]. EP TOMS was also able to detect passive volcanic degassing of Popocatepetl volcano, Mexico, when operated in a one-time low-orbit, stare mode configuration in 1997 [11]. However, the 4–6 DU SO_2 noise levels in the vertical column (1 Dobson unit (DU) $= 2.69 \times 10^{16}$ molecules/cm^2) are too high to measure background SO_2 amounts or most anthropogenic SO_2 [12]. Greatly improved sensitivity was demonstrated through detection of volcanic and anthropogenic SO_2 in Global Ozone Monitoring Experiment (GOME) and SCIAMACHY full spectrum UV data [13]–[15]. However, these sensors need several days to acquire a contiguous global map and hence could miss short-lived pollution events. Infrared detection of volcanic SO_2 has also been demonstrated with Atmospheric Infrared Sounder (AIRS) data [16], but IR sensors have low sensitivity to tropospheric and boundary layer SO_2 emissions.

The NASA EOS Aura platform [17], launched on July 15, 2004, carries the Ozone Monitoring Instrument (OMI) [18], a hyperspectral UV/Visible spectrometer with a 2600 km swath for daily, global contiguous mapping that was provided by the Netherlands Agency for Aerospace Programs (NIVR) in collaboration with the Finnish Meteorological Institute (FMI) to the NASA EOS Aura mission for continued monitoring of ozone and other trace gases [19]. The Royal Netherlands Meteorological Institute (KNMI) is the Principal Investigator institute. Reflected sunlight in a fan-shaped narrow field of view is dispersed by a spectrometer and imaged in spatial–spectral dimensions on two-dimensional charge coupled device (CCD) detectors, one for UV and one for visible bands [20]. We use data from the 310–365 nm UV-2 band of OMI with spectral resolution of ~ 0.4 nm [18], [20]. Data are collected from the pushbroom swath in 2-second intervals corresponding to 13-km along-track resolution. Pixels are binned in 60 cross-track positions to provide a nadir resolution of 24 km. A solar calibration is taken at the northern terminator [21].

Currently, calibrated radiances are routinely produced for 12 UV2 OMI wavelengths for operational production of TOMS-like column ozone (OMTO3), SO_2 data (OMSO2) and vicarious calibrations [22], [23]. We have developed a new technique termed the band residual difference (BRD) algorithm that utilizes four of these wavelengths that are positioned at SO_2 band extrema between 310.8 and 314.4 nm. Being less computationally demanding than the spectral fitting maximum likelihood (ML) algorithm [24], the BRD method is also faster and applicable to generation of OMI SO_2 data in a near-real time operational scenario (e.g., for volcanic cloud advisories to aviation). The BRD algorithm used to produce initial Level 2 SO_2 data until such a time as the ML method can be implemented. This paper describes the BRD algorithm and includes examples of preliminary OMI SO_2 retrievals.

Manuscript received April 29, 2005; revised September 28, 2005. This work was supported in part by NASA under OMI and TOMS science teams.

N. A. Krotkov is with the Goddard Earth Sciences and Technology Center, University of Maryland Baltimore County, Baltimore, MD 21228 USA (e-mail: krotkov@chescat.gsfc.nasa.gov).

S. A. Carn and A. J. Krueger are with the Joint Center for Earth System Technology, University of Maryland Baltimore County, Baltimore, MD 21250 USA (e-mail: scarn@umbc.edu, akrueger@umbc.edu).

P. K. Bhartia is with the Laboratory for Atmospheres, NASA Goddard Space Flight Center,Greenbelt, MD 20771 USA (e-mail: Pawan.Bhartia@nasa.gov).

K. Yang is with Science Systems and Applications, Inc., Lanham, MD 20706 USA (e-mail: Kai.Yang.1@gsfc.nasa.gov).

Digital Object Identifier 10.1109/TGRS.2005.861932

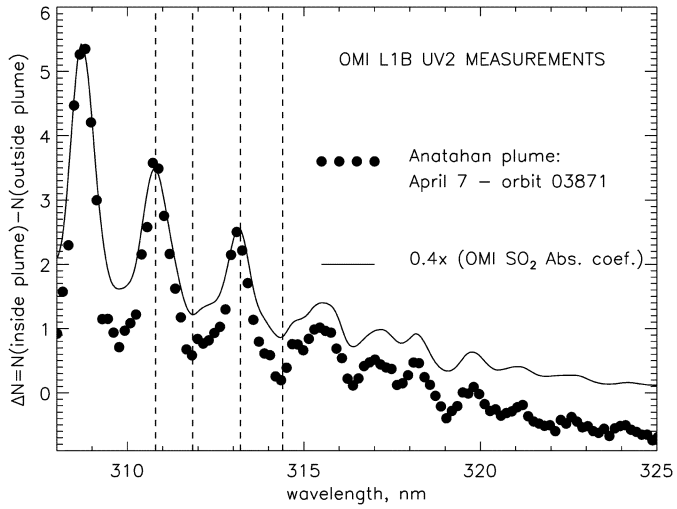

Fig. 1. OMI measured N-value spectra difference inside and outside the Anatahan volcanic plume on April 7, 2005 (orbit 3871) overlapped with a scaled SO_2 cross section [25] smoothed with the nominal OMI UV-2 slit function (triangular, $\mathrm{FWHM} = 0.45$ nm [18]). Nadir observational direction, solar zenith angle 23°, $\mathrm{LER} = 0.1$.

II. OMI SO_2 Algorithm

A. Algorithm Overview

The BRD algorithm makes use of OMTO3 ozone, Ω_T, Lambertian effective reflectivity (LER), and calibrated residuals at four UV-2 wavelengths centered on SO_2 bands (Fig. 1) to estimate a total vertical column SO_2 amount, Σ_o assuming that the logarithm of the spectral reflectance ratio in wavelength pairs can be approximated as

$$N_j = \mathrm{kmg}_j(\alpha_j\Omega_o + \gamma_j\Sigma_o) + \frac{\partial S}{\partial\lambda}\Delta\lambda_j \tag{1}$$

where Ω_o and Σ_o are true column ozone and SO_2 amounts, $N_j = N\left(\lambda_j^{\mathrm{short}}\right) - N\left(\lambda_j^{\mathrm{long}}\right)$ is the measured N-pair value $(N = -100 * \log_{10}(I/F))$ where I is Earth radiance and F is solar irradiance) for wavelength pair p_j, $j = 1, 2, 3$, and γ_j and α_j are SO_2 and O_3 differential absorption coefficients for the pair; $m = \sec\theta_o + \sec\theta$ is the geometrical air mass factor (AMF); relative column average photon path of sunlight entering the atmosphere at solar zenith angle θ_o and exiting the atmosphere at the OMI viewing zenith angle θ; g_j is a correction to m accounting for absorber vertical distribution, column amount and LER (see Sections II-C and D); $k = 100/\ln 10$ is a scaling factor and the $S(\lambda)$ term represents any systematic biases in either the measurements (calibration) or the model as well as the scattering atmospheric contribution. The main advantage of using pair N values is that wavelength-independent systematic errors are cancelled and wavelength-dependent error terms become proportional to $\Delta\lambda_j$; the latter is minimized by selecting close wavelength pairs: $\Delta\lambda_j \to 0$ (Fig. 1).

Table I shows the pair wavelengths currently used by the BRD algorithm, and differential 225 K ozone and 295 K SO_2 absorption coefficients [25]. Fig. 1 shows an analysis of OMI UV-2 spectra from a SO_2 cloud discharged by Anatahan volcano (16.35°N, 145.67°E; Mariana Islands) on April 6, 2005. Using a pixel within the April 7, 2005 Anatahan cloud (lat: 14.34°N) and a cloud-free pixel from the same scan position (31—nadir) we obtain an OMI observed differential N-value spectrum to compare with a lab spectrum of SO_2 [25] with band center wavelengths from Table I. The SO_2 spectral band positions agree to within 0.1 nm, thus confirming the OMI wavelength calibration [20], [21].

TABLE I
OMI SO_2 Pair Differential Cross Sections (Smoothed With the OMI Slit Function, Triangular $\mathrm{FWHM} = 0.45$ nm)

Pair	λ^{short} - λ^{long}, [nm]	Pair differential absorption coefficients [atm-cm^{-1}]	
		Ozone: α_j	SO_2: γ_j
P_1	310.8 - 311.9	0.29	5.65
P_2	311.9 - 313.2	0.34	-3.3
P_3	313.2 - 314.4	0.27	4.16
P_B	317.6 - 331.3	0.76	1.97

Equation (1) can be applied to the operational OMTO3 ozone retrieval. The OMTO3 algorithm [22], [23] retrieves the total ozone amount, Ω_T and Lambertian Equivalent surface Reflectivity (LER) using the B-pair: $P_B = (317.6\ \mathrm{nm},\ 331.3\ \mathrm{nm})$ under most conditions, and the C-pair: $P_C = (331.3\ \mathrm{nm},\ 360.2\ \mathrm{nm})$ for high ozone and high solar zenith angle conditions. The longer of the two wavelengths is used to derive LER (or cloud fraction); the shorter wavelength provides total ozone. The residuals at the ten other wavelengths are then calculated as the difference between the measured and the computed N-values that account for the effects of multiple Rayleigh scattering, ozone absorption, Ring effect, and surface reflectivity. Using the B-pair and assuming that ozone is the only absorber

$$N_B = \mathrm{kmg}_B\alpha_B\Omega_T + \frac{\partial C}{\partial\lambda}\Delta\lambda_B. \tag{2}$$

In (2), both Ω_T and $(\partial C/\partial\lambda)\Delta\lambda_B$ provide closure between the measured and calculated B-pair N values [22], [23]. If SO_2 is present, Ω_T represents the combined effective column absorber amount

$$\Omega_T = \Omega_o + \frac{\gamma_B}{\alpha_B}\Sigma_o \tag{3}$$

where Ω_o and Σ_o are the true column ozone and SO_2 amounts. The OMTO3 algorithm next uses retrieved values of Ω_T and LER to calculate residual N values $\mathrm{res}_j = N_j^{\mathrm{measured}} - N_j^{\mathrm{calculated}}$ at SO_2 wavelength pairs: $p_J, j = 1, \ldots, 3$. (Table I). In our notation, the $N_j^{\mathrm{calculated}}$ can be represented similarly to (1)

$$N_j^{\mathrm{calculated}} = \mathrm{kmg}_j\alpha_j\Omega_T + \frac{\partial C}{\partial\lambda}\Delta\lambda_j. \tag{4}$$

In the presence of SO_2, shorter wavelength pair residuals are strongly correlated with the differential SO_2 cross section and can be used for SO_2 estimation [22]. The equation for residuals is obtained by subtracting (4) from (1) and accounting for (3)

$$\begin{aligned}\mathrm{res}_j &= N_j - N_j^{\mathrm{calculated}}(\Omega_T, \mathrm{LER}) \\ &= \mathrm{kmg}_j\Sigma_o\gamma_j\left[1 - \frac{\alpha_j}{\gamma_j}\frac{\gamma_B}{\alpha_B}\right] + \mathrm{bias}.\end{aligned} \tag{5}$$

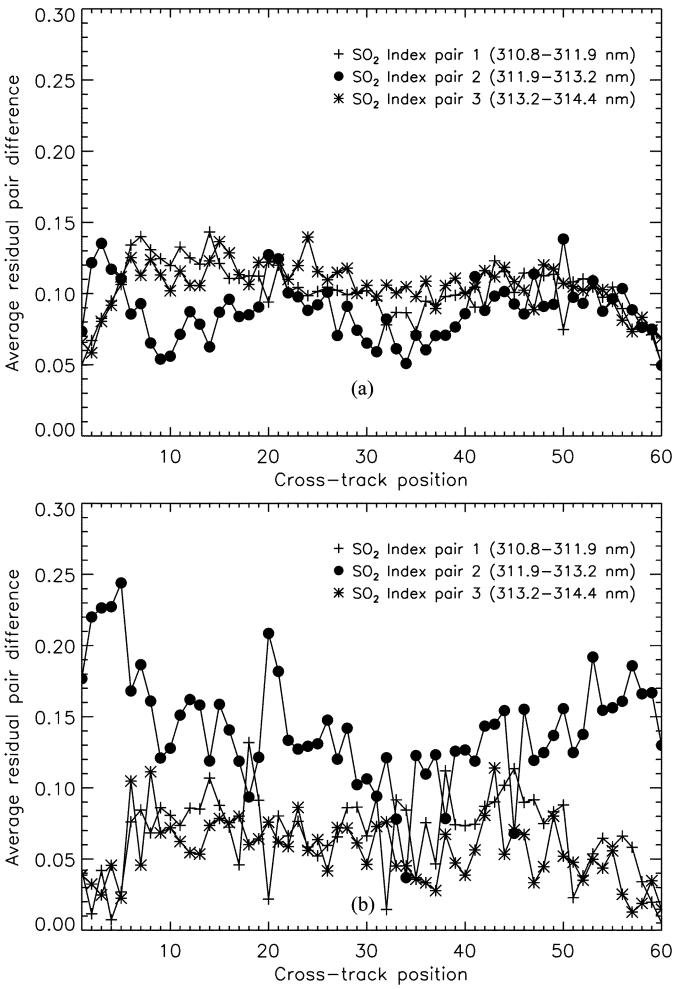

Fig. 2. Global equatorial pair residuals (daily average biases for each cross-track pixel within 20° latitude of the equator) on (a) March 28, 2005 and (b) August 30, 2005.

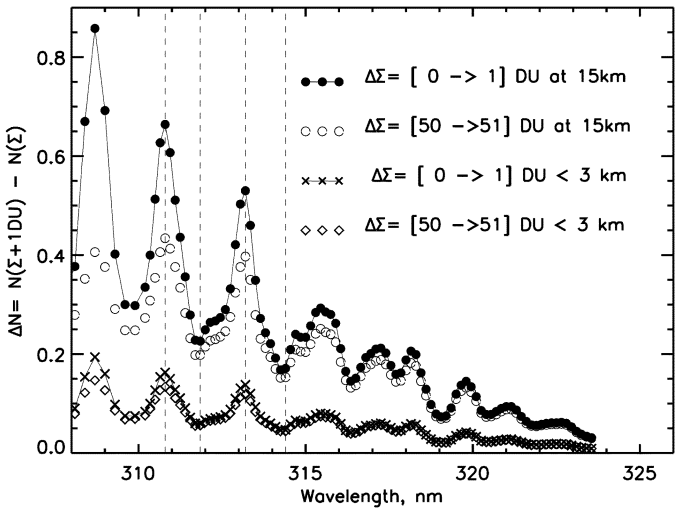

Fig. 3. Modeling of incremental effect of 1 Dobson Unit ($1\ \mathrm{DU} = 2.69 \times 10^{16}$ molecules/cm^2) of SO_2 on spectral N-values ($N = -100 \log 10(I/F)$) at the top of the atmosphere. SO_2 was placed at 15 km (upper 2 curves represent small (1 DU) and high (50 DU) SO_2 loading) and in the boundary layer (lower curve). The N-values were smoothed with the OMI triangular slit function ($\mathrm{FWHM} = 0.45$ nm). OMTO3 SO_2 residual wavelengths (Table I) are shown as dashed lines. The assumptions used in RT calculations: Nadir observational direction, overhead sun, LER [22], [23]: $\mathrm{LER} = 0.05$.

B. Background Corrections

Biases resulting from nonperfect instrument calibration as well as from forward model simplifications are empirically corrected. Fig. 2 shows examples of the cross-track variation of global equatorial pair residuals (the average bias for each cross-track position (constant viewing zenith angle, θ) within $\pm 20^\circ$ latitude of the equator, calculated after excluding heavily SO_2-contaminated pixels and their variation over time. Biases are corrected by subtracting equatorial pair residuals from the raw pair values for each OMI orbit.

Following the equatorial bias correction SO_2 amounts can be analytically estimated from the single wavelength pair residual given by (5)

$$\Sigma_j = \frac{\mathrm{res}_j(\Sigma) - \langle \mathrm{res}_j(\mathrm{Equatorial}) \rangle_{\theta=\mathrm{const}}}{k(\sec\theta + \sec\theta_o) g_j(H_\Sigma, \Sigma) \gamma_j \left[1 - \frac{\alpha_j}{\gamma_j} \frac{\gamma_B}{\alpha_B}\right]}. \quad (6)$$

Using three different OMTO3 pair residuals, one obtains independent estimates of SO_2 vertical column amounts within the same OMI pixel: Σ_j. These are further averaged to produce the operational SO_2 vertical column amount. The differences between individual Σ_j estimates are also written to the output file to provide a useful indicator of the overall accuracy of the OMI measurements and the BRD algorithm assumptions.

C. Air-Mass Corrections Due to SO_2 Height and Amount

Initial SO_2 estimates could be made assuming a geometrical AMF [$g_j = 1$ in (6)]. However, a geometrical approximation to the AMF ($m = \sec\theta_o + \sec\theta$) is a simplification because of atmospheric scattering and absorption as well as surface reflection. The approximation fails for low sun elevations because of Earth sphericity. Clouds and aerosols in the boundary layer also affect the AMF in complicated ways. For large SO_2 amounts, using a geometrical AMF will underestimate the SO_2 load, due to a reduced UV-light penetration effect. The effect depends on wavelength, reflectivity, observational geometry, SO_2 load and vertical profile. Fig. 3 illustrates the saturation effect for the most favorable observational conditions: overhead sun, nadir view angle, 325 DU standard ozone profile [22], [23], with no clouds or aerosol scattering. The SO_2 vertical profiles were assumed to be Gaussian for a volcanic cloud at 15 km (with 1 km standard deviation) and uniform mixing between the surface and 3 km (700 mb) for the boundary layer case.

For more accurate consideration each absorption coefficient in (1)–(6) at each wavelength should be multiplied by its own effective AMF that depends also on the absorber amount and profile. In doing so, the equations become nonlinear in absorber amounts and the retrieval problem becomes circular: the AMFs are required for column amounts estimates, but AMFs themselves require prior knowledge of absorber amounts. However, first-order corrections to the geometrical AMF approximation, g can be estimated using offline forward RT calculations [26]

$$g_j = \frac{10^3}{\mathrm{km}\gamma_j} \frac{\Delta N_j}{\Delta\Sigma} \quad (7)$$

where ΔN_j is the pair N_j value increment due to a small column SO_2 change (assuming fixed SO_2 profile, reflectivity and ge-

TABLE II
CORRECTION FACTORS TO GEOMETRICAL AMF FOR 5% SURFACE REFLECTIVITY AND 325 DU MID-LATITUDE OZONE PROFILE [22], [23], OVERHEAD SUN, AND NADIR VIEWING DIRECTION, NO AEROSOL OR CLOUDS

SO_2 Column amount	SO_2= 0 - 10 DU		SO_2=50-60DU	
Plume height	<3 km	15km	< 3km	15km
P1	0.21	0.89	0.16	0.48
P2	0.27	1.06	0.22	0.70
P3	0.25	0.99	0.21	0.68

ometry) and γ_j is the differential SO_2 absorption coefficient (atm-cm^{-1}) at wavelength pair p_j. The N_j values were calculated with a forward RT model assuming different SO_2 loads and vertical profiles (Fig. 3). The g_j factors were calculated from (7) for different wavelength pairs P_1–P_3. As can be seen from Table II, g factors are close to 1 only for upper tropospheric/stratospheric plumes containing small SO_2 loads ($<$10 DU). Fresh stratospheric plumes typically have much larger SO_2 loads ($>$50 DU), in which case g is greatly reduced ($\sim$0.5–0.7) due to the reduced penetration of UV light. On the other hand, for small SO_2 sources that are expected to produce plumes in the boundary layer, the g factor is $\sim$0.2–0.3, due to the penetration effect, especially at shorter UV wavelengths (Table II). The penetration problem is exacerbated at large solar zenith angles and large view angles (off-nadir pixels) as well as for increased ozone amounts. Therefore, the detection of small SO_2 plumes becomes more challenging for middle and high latitudes. In any case, both the SO_2 altitude and load should be known approximately beforehand to allow reasonable AMF corrections. The whole problem could then be solved iteratively by assuming a geometric air-mass factor as a first step, then calculating SO_2 amounts from (6) and AMF corrections from (7) (or interpolated g values from Table II), then recalculating SO_2 amounts from (6) and estimating g and so on. However, the SO_2 vertical profile should be known (or estimated) from ancillary sources.

The g factors given in Table II apply to the most favorable observational scenario: overhead sun, nadir viewing position, no aerosols or clouds. However, the impact of solar zenith angle (less than 70°) and viewing geometry (viewing angle less than 70° and azimuthal angle $\sim$ 90°) on the volcanic AMF is reasonably well represented by the geometrical approximation (m). Therefore, the g factors in Table II are applicable to all clear pixels not far off-nadir with moderate solar zenith angles in low and middle latitudes. These cases can be easily identified in OMI data by looking at low reflectivity pixels. We concentrate on such clear cases first (see Section III).

D. AMF Corrections Due to Underlying Reflectivity

The sensitivity of backscattered radiances to SO_2 increases with increasing reflectivity of the underlying surface [26]. Although enhanced surface reflectivity assists detection of small SO_2 plumes, especially those in the planetary boundary layer (PBL) that otherwise are undetectable by OMI, it will also produce overestimates of actual SO_2 loading if the AMF is not adjusted. Table III compares g factors at $\mathrm{LER} = 5\%$ (Table II) and $\mathrm{LER} = 80\%$. We note that the largest increase in SO_2 sensitivity occurs for PBL SO_2 (up to factor of 5), while for stratospheric volcanic plumes sensitivity increases by only $\sim$30%.

TABLE III
RATIO OF CORRECTION FACTORS FROM $\mathrm{LER} = 80\%$ TO $\mathrm{LER} = 5\%$

SO_2 Column amount	SO_2= 0 - 10 DU		SO_2=50 - 60DU	
Plume Heigt	<3 km	15km	< 3km	15km
P1	4.8	1.2	4.5	1.5
P2	4.7	1.1	4.5	1.3
P3	4.7	1.1	4.5	1.3

The OMI total ozone algorithm (OMTO3) output file includes LER at 331 nm. We correct g factors by interpolating values given in Table III to the actual OMI measured value of LER.

III. OMI SO_2 DATA OVERVIEW

The OMI SO_2 product (OMSO2) uses the HDF5-EOS format. Each OMSO2 granule corresponds to a single OMI orbit. In addition to standard geolocation and satellite ephemeris parameters, the OMSO2 product contains the residual pair difference values (N_j); total column SO_2 for three different SO_2 cloud altitudes (PBL, 5 km, and 15 km); OMTO3 aerosol index, ozone, and reflectivity values [22]; and data quality flags.

A. Explosive Eruptions

The AURA OMI SO_2 volcanic data set will continue the TOMS SO_2 record, which covers a quarter-century [1]–[7].[1] Using the BRD algorithm, we have been able to measure SO_2 emissions from every significant volcanic eruption that has occurred since OMI data became routinely available in September 2004. One example, the eruption of Manam volcano (Papua, New Guinea) on January 27–28, 2005, can be seen in [27]. Fig. 4 shows SO_2 emissions produced by an eruption of Anatahan volcano (Mariana Islands) on April 6 (this cloud was used for the analysis shown in Fig. 1). The high sensitivity and contiguous coverage of OMI allows such emissions to be tracked for several days, providing opportunities for trajectory model validation.

Very few events remain undetected by OMI; the main factors impeding detection of lower tropospheric SO_2 emissions are extensive cloud cover and/or high ozone column amounts (both common over the volcanoes of Russia's Kamchatka Peninsula, for example). The latter can overwhelm the SO_2 absorption in lower tropospheric volcanic clouds (also see Section IV).

OMI's high sensitivity to SO_2 also permits one to conclude with more confidence whether an explosive eruption has produced SO_2 or if it has not (i.e., if it is a phreatic, or steam-driven event). This is very important in an aviation hazards context, since production of SO_2 indicates a magmatic eruption with the potential for buoyant upper tropospheric or stratospheric (i.e., aircraft cruising level) plumes.

B. Passive Degassing

The OMI BRD algorithm has permitted the first daily, space-based measurements of passive volcanic SO_2 degassing (e.g.,

[1]http://toms.umbc.edu.

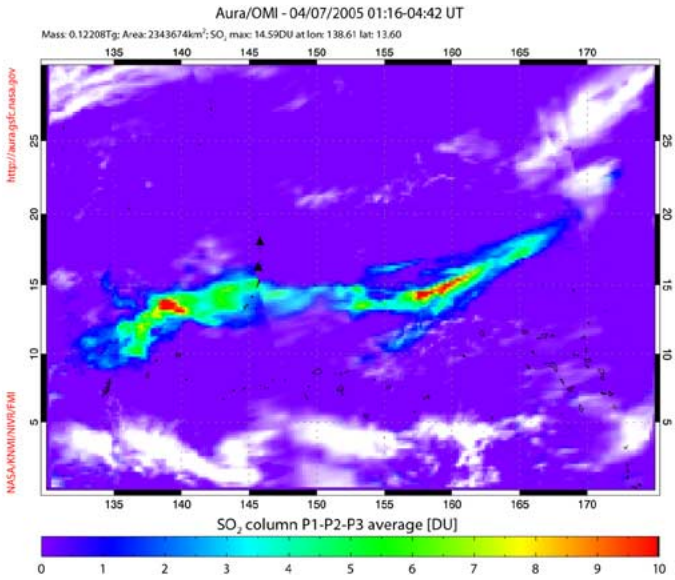

Fig. 4. OMI SO_2 image of the Anatahan (16.35°N, 145.67°E) eruption cloud on April 7, 2005, produced by an explosive eruption on April 6. White regions are meteorological clouds.

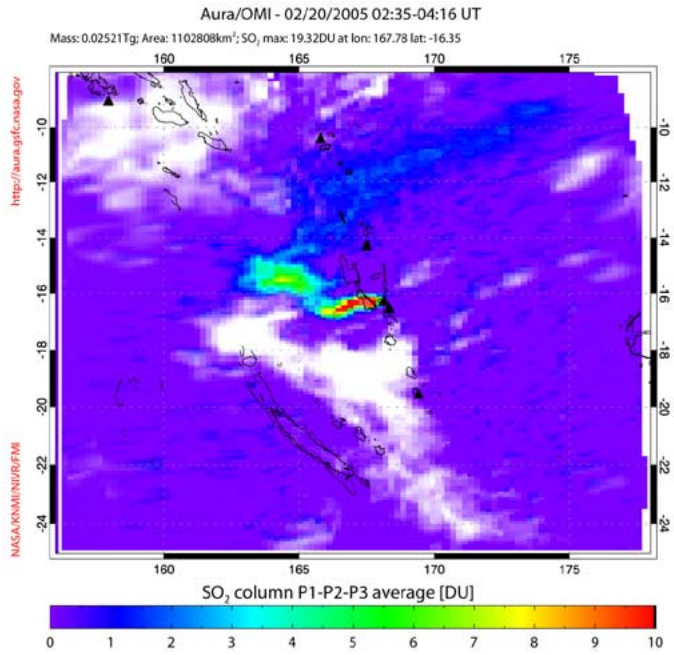

Fig. 5. OMI SO_2 image of passive degassing from Ambrym volcano, Vanuatu (16.25°S, 168.12°E) on February 20, 2005. White regions are meteorological clouds.

[28], [29]) in the lower troposphere. Strong SO_2 sources (e.g., [29]; Fig. 5) can be tracked on a daily basis with OMI (in the absence of significant cloud cover), whilst for weaker sources a successful approach has been to generate weekly or monthly averages of OMI SO_2 data to increase the signal to noise ratio (e.g., [29]).

C. Anthropogenic SO_2 Pollution

We have also achieved very promising measurements of anthropogenic SO_2 emissions using the BRD algorithm. SO_2 emissions have been measured by OMI over known sources

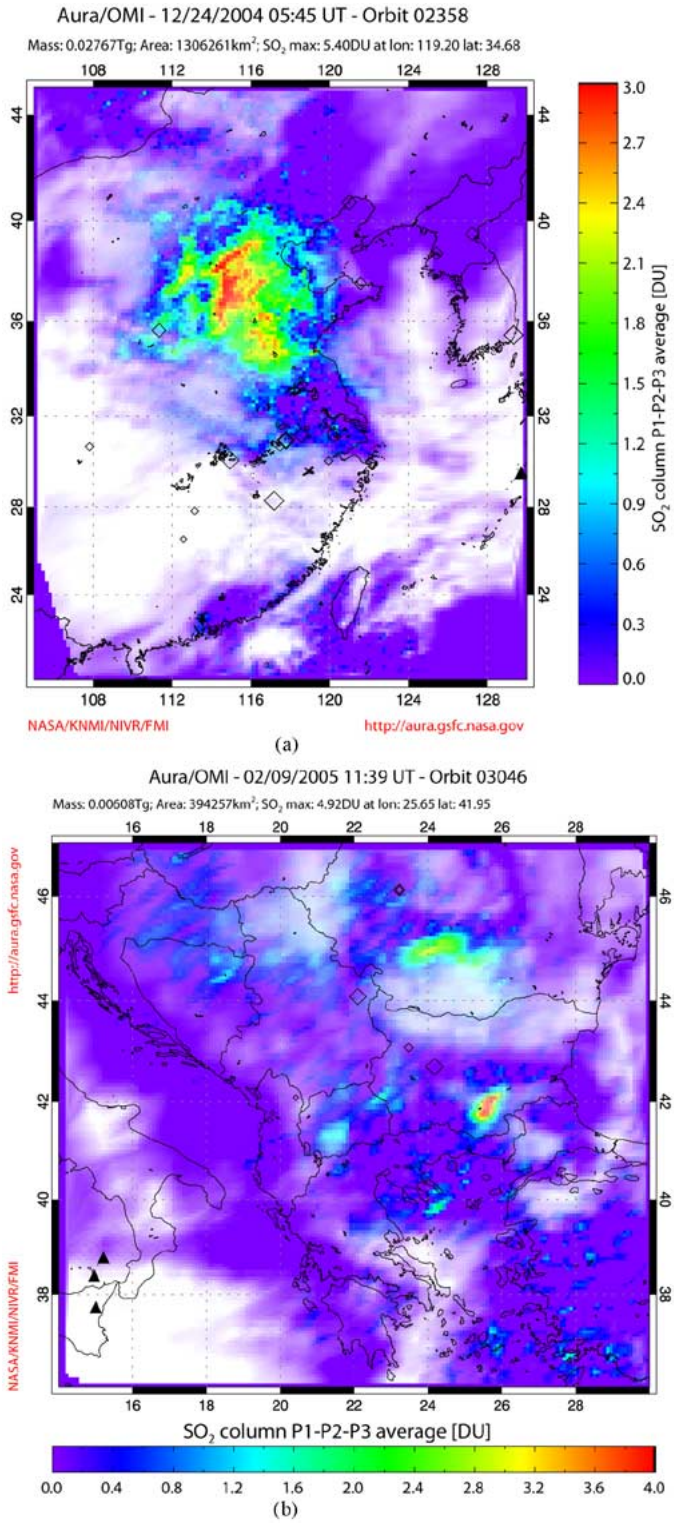

Fig. 6. OMI measurements of anthropogenic SO_2 emissions in the PBL. (a) Air pollution in a cloud-free region of eastern China on December 24, 2004. Clouds are shown in white. (b) SO_2 emissions from sources in S.E. Europe (chiefly in Romania and Bulgaria) on February 9, 2005. Note the low background noise (< 0.5 DU) in both images.

of air pollution, such as the Ohio valley in the U.S., Eastern China, and Eastern Europe (e.g., Fig. 6). The most significant discovery to date has been the detection of SO_2 emissions from individual copper smelters in South America and elsewhere. These measurements will be discussed in a separate paper [30].

TABLE IV
OMI SO_2 BACKGROUND NOISE ESTIMATION

Region	Mean, DU	Standard deviation, DU
North Atlantic, January 2005, PBL SO_2	-0.066	0.50
South Pacific, January 2005, SO_2 cloud at 15 km	-0.050	0.22

Fig. 6 shows OMI SO_2 retrievals in polluted regions of eastern Asia and Eastern Europe. These examples show that OMI can observe SO_2 emissions in the PBL on a daily basis, thereby improving on GOME and SCIAMACHY, which need several days to acquire a contiguous global map [13]–[15] and hence could miss short-lived pollution events. We note that the SO_2 enhancements detected by OMI in Eastern Europe in February 2005 (Fig. 6(b)) correspond in both location and approximate column amount to GOME observations from February 1998 reported in [14]. These SO_2 emissions are sourced from lignite-burning power plants in the Balkan region [14].

IV. DATA QUALITY ASSESMENT

Assessment of OMI data quality is difficult as minimal SO_2 validation data are currently available. Errors will not necessarily be randomly distributed over the globe, but will typically increase with solar zenith angle, large ozone, or SO_2 column amounts and in the presence of clouds and heavy aerosol loading.

With a lifetime of about a day in the lower troposphere, the amount of SO_2 in the PBL is typically very small (less than 0.5 DU except very near to a source). In nonpolluted regions, including most of the Southern hemisphere, the amount is near zero. Thus, the retrieval sensitivity can be estimated from the noise level in background areas. An initial evaluation for two assumed SO_2-free regions, over the N. Atlantic (40–60°N, 10–45°W) and S. Pacific (0–40°S, 120–180°W) in January 2005, produces the results shown in Table IV. The N. Atlantic case assumes a boundary layer SO_2 profile and is applicable to a pollution scenario at midlatitudes in winter. The S. Pacific example is for a volcanic SO_2 cloud at 15 km and, therfore, shows the noise expected under optimum retrieval conditions (overhead sun, upper tropospheric/stratospheric SO_2 cloud).

We, therfore, expect the standard deviation of OMI SO_2 retrievals to be 0.5 DU or less, which is ten times lower than TOMS SO_2 data [4]–[6].

When SO_2 is present, the retrieval depends on its vertical distribution and total amount. As most air pollution sources release the SO_2 into the PBL or lower troposphere, we assume a constant mixing ratio distribution in the PBL. The height of the PBL is currently assumed to be 3 km (700 mb), but in the future it could also be specified either from external data or from climatology. As the retrieval dependence on altitude becomes small in the upper troposphere and stratosphere, we assume that eruption clouds are at 15 km (close to the tropopause in the tropics, where most explosive eruptions occur). Passive emissions frequently take place from volcanic vents that release SO_2 into the free troposphere. We initially assume this occurs near 5 km.

The largest errors are expected for cloudy and partially cloudy conditions. Depending on their location relative to the SO_2, meteorological clouds can shield SO_2 at low altitudes from OMI, or artificially enhance the SO_2 signal above them. In addition, there is a small positive bias associated with reflective meteorological clouds, which produce a bias typically on the order of 0.2 DU SO_2 but up to $\sim$1 DU in some cases. The bias is most apparent at the edges of clouds, or in the presence of small (subpixel sized), highly reflective clouds.

In polluted regions the sulfate haze from oxidation of older SO_2 constitutes a source of error in the retrievals if not accounted for in the atmospheric model used in AMF estimation. Retrieval errors arise from noise in the radiance measurements, and from simplifications in the atmospheric models and in cross section data. Ash in volcanic clouds can produce as much as 30% error if not accounted for in the AMFs [4], [6], [26]. Passive emissions typically have less than 50 DU SO_2 and are often free of ash so that no error occurs due to ash.

V. SO_2 VALIDATION PLAN

Comparisons of OMI with Earth Probe TOMS data for explosive eruption clouds are needed to assure consistency between the databases for extension of the TOMS eruption SO_2 mass time series. EP TOMS operations are planned for at least 2 years overlap with OMI.

Subsequently, we plan to compare OMI total column SO_2 with AURA Microwave Limb Sounder (MLS) SO_2 measurements. The advantage of such comparisons is that MLS provides the vertical distribution of SO_2 in the stratosphere and upper troposphere (down to 215 hPa) [31]. Using this information we will be able to specify the profile for the AMF g_j in (7).

In addition to MLS, other A-Train sensors are capable of measuring SO_2 and will provide coincident or near-coincident correlative observations for validation of OMI SO_2 data. On Aura, the Tropospheric Emission Spectrometer (TES)[2] has IR channels suitable for SO_2 measurements. TES is a pointable Fourier Transform Spectrometer capable of tropospheric SO_2 profile retrievals in limb or nadir viewing mode. On Aqua, the IR AIRS instrument offers high sensitivity to SO_2 and a similar footprint dimension to OMI ($\sim$13.5 km) [16], and is, therfore, an important source of correlative observations. However, due to interference from water vapor AIRS is typically unable to provide correlative measurements of SO_2 in the PBL or lower troposphere. Preliminary comparisons of OMI SO_2 data with AIRS and EP-TOMS data for explosive eruptions show that OMI SO_2 columns are accurate for upper tropospheric SO_2 clouds.

The Moderate Resolution Imaging Spectroradiometer (MODIS) on Aqua also has IR channels sensitive to SO_2. Although MODIS is inherently less sensitive to SO_2 than AIRS or OMI, its high spatial resolution (1 km) will provide information on SO_2 variability and/or meteorological cloud interference on sub-OMI pixel scales. This will be particularly important for evaluation of OMI SO_2 retrievals in the PBL.

Validation of OMI measurements of SO_2 located in the lower troposphere and PBL is more challenging. We plan to use low-altitude aircraft SO_2 measurements (spirals) [12] as well as ground-based column SO_2 measurements from double

[2]http://tes.jpl.nasa.gov

TABLE V
COMPARISON OF SO_2 DETECTION LIMITS FOR ERUPTION CLOUDS AT OR ABOVE 15 km FROM TOMS AND OMI

Instrument	Typical noise level, DU	Nadir footprint area, km^2	Detection limit, tons 5 pixels@ 5 σ
TOMS	5	2500	7000
OMI	0.22	312	47

Brewer spectrometer stations and portable UV spectrometers near SO_2 sources. The latter endeavor will be facilitated by the current proliferation of compact UV spectrometers in the volcanological community (e.g., [32]), which is improving the quantity and temporal resolution of ground-based differential optical absorption spectroscopy (DOAS) measurements of SO_2 at degassing volcanoes. The OMI validation effort will benefit from the imminent deployment of a global network of these instruments [33].

VI. CONCLUSION

Almost a quarter-century of TOMS volcanic eruption SO_2 masses are now available [6]–[7]. The OMI SO_2 data set will continue the TOMS record but the improved sensitivity and smaller footprint of OMI will extend the range of detection to smaller eruptions and older clouds, and to degassing volcanoes. A comparison of the volcanic cloud detection capability for TOMS and OMI is shown in Table V. A conservative cloud detection algorithm requires five adjacent pixels each containing more than five noise standard deviations. A dramatic 150-fold improvement is found.

Using OMI data, we can directly compare daily global SO_2 emissions from anthropogenic and volcanic sources for the first time, and thus provide important new constraints on the relative magnitude of these fluxes. Such measurements are essential given the growing concern over the effects of anthropogenically forced climate change and intercontinental transport of air pollution. The fast BRD SO_2 retrieval is also amenable to operational SO_2 alarm development, and near real-time application for aviation hazards and volcanic eruption warnings.

The BRD algorithm sensitivity does not represent the maximum sensitivity theoretically achievable with OMI and, hence, future algorithm improvements should allow even weaker SO_2 sources to be monitored routinely. These measurements are expected to produce the best estimates to date of the volcanic contribution to global atmospheric SO_2 abundances.

ACKNOWLEDGMENT

The authors would like to thank the KNMI OMI team for producing L1B radiance data and the U.S. OMI operational team for continuing support. They also appreciate the work of D. Flittner for help with radiative transfer calculations and thank G. Bluth and a second anonymous reviewer for suggesting improvements to the paper. They also thank P. Levelt and J. de Haan (KNMI) and J. Tamminen (FMI) for their thorough reading of the manuscript and valuable comments.

REFERENCES

[1] A. J. Krueger, "Sighting of EL Chichon sulfur dioxide clouds with the Nimbus 7 total ozone mapping spectrometer," *Science*, vol. 220, pp. 1277–1379, 1983.
[2] G. J. S. Bluth, S. D. Dorion, C. C. Schnetzler, A. J. Krueger, and L. S. Walter, "Global tracking of the SO_2 clouds from the Mount Pinatubo eruptions," *Geophys. Res. Lett.*, vol. 19, no. 2, pp. 151–154, Jun. 1992.
[3] ——, "The contribution of explosive volcanism to global atmospheric sulfur dioxide concentrations," *Nature*, vol. 366, pp. 327–329, 1993.
[4] A. J. Krueger, L. S. Walter, P. K. Bhartia, C. C. Schnetzler, N. A. Krotkov, I. Sprod, and G. J. S. Bluth, "Volcanic sulfur dioxide measurements from the total ozone mapping spectrometer instruments," *J. Geophys. Res.*, vol. 100, no. D7, pp. 14 057–14 076, 1995.
[5] C. C. Schnetzler, G. S. J. Bluth, A. J. Krueger, and L. S. Walter, "A proposed volcanic sulfur dioxide index (VSI)," *J. Geophys. Res.*, vol. 102, pp. 20 087–20 092, 1997.
[6] A. J. Krueger, S. J. Schaefer, N. Krotkov, G. Bluth, and S. Barker, "Ultraviolet remote sensing of volcanic emissions," in *Remote Sensing of Active Volcanism, Geophys. Monogr. Ser.*, P. J. Mouginis-Mark, J. A. Crisp, and J. H. Fink, Eds. Washington, D.C.: AGU, 2000, vol. 116, pp. 25–43.
[7] S. A. Carn, A. J. Krueger, G. J. S. Bluth, S. J. Schaefer, N. A. Krotkov, I. M. Watson, and S. Datta, "Volcanic eruption detection by the Total Ozone Mapping Spectrometer (TOMS) instruments: A 22-year record of sulphur dioxide and ash emissions," in *Volcanic Degassing, Spec. Public Geolog. Soc. London*, C. Oppenheimer, D. M. Pyle, and J. Barclay, Eds. London: Geological Society, 2003, vol. 213, pp. 177–202.
[8] G. S. Gurevich and A. J. Krueger, "Optimization of TOMS wavelength channels for ozone and sulfur dioxide retrievals," *Geophys. Res. Lett.*, vol. 24, no. 17, pp. 2187–2190, 1997.
[9] S. A. Carn, "Eruptive and passive degassing of sulfur dioxide at nyiragongo volcano (D.R. Congo): The 17 January 2002 eruption and its aftermath," *Acta Vulcanologica*, vol. 14–15, pp. 75–86, Jan. 2004.
[10] S. A. Carn, N. A. Krotkov, M. A. Gray, and A. J. Krueger, "Fire at Iraqi sulfur plant emits SO_2 clouds detected by earth probe TOMS," *Geophys. Res. Lett.*, vol. 31, 2004.
[11] S. J. Schaefer, J. B. Kerr, M. M. Millan, V. J. Realmuto, A. J. Krueger, N. A. Krotkov, C. Seftor, and I. E. Sprod, "Geophysicists unite to validate volcanic SO_2 measurements," *EOS Trans. Amer. Geophys. Union*, vol. 78, no. 217, pp. 223–223, 1997.
[12] Joint Assembly Suppl., Abstract A31D-02, [Online]. Available: http://www.agu.org/cgi-bin/sessionssm04?meeting=sm04∂=A31D=200R. R. Dickerson, J. C. Hains, and J. P. Burrows, "Combining *in situ* and remote measurements with models: Picking the right tools," *EOS Trans. Amer. Geophys. Union*, vol. 85, no. 17, 2004.
[13] J. P. Burrows, M. Weber, M. Buchwitz, V. Rozanov, A. Ladstätter-Weissenmayer, A. Richter, R. de Beek, R. Hoogen, K. Bramstedt, K.-U. Eichmann, M. Eisinger, and D. Perner, "The Global Ozone Monitoring Experiment (GOME): Mission concept and first scientific results," *J. Atmos. Sci.*, vol. 56, pp. 151–175, 1999.
[14] M. Eisinger and J. P. Burrows, "Tropospheric sulfur dioxide observed by the ERS-2 GOME instrument," *Geophys. Res. Lett.*, vol. 25, pp. 4177–4180, 1998.
[15] H. Bovensmann *et al.*, "SCIAMACHY—Mission objectives and measurement modes," *J. Atmos. Sci.*, vol. 56, pp. 127–150, 1999.
[16] S. A. Carn, L. L. Strow, S. de Souza-Machado, Y. Edmonds, and S. Hannon, "Quantifying tropospheric volcanic emissions with Airs: The 2002 eruption of Mt. Etna (Italy)," *Geophys. Res. Lett.*, vol. 32, 2005.
[17] M. R. Schoeberl, A. R. Douglass, E. Hilsenrath, P. K. Bhartia, J. Barnett, J. Gille, R. Beer, M. Gunson, J. Waters, P. F. Levelt, and P. DeCola, "Earth Observing System misions benefit atmospheric research," *EOS Trans. Amer. Geophys. Union*, vol. 85, no. 18, pp. 177–181, May 2004.
[18] P. F. Levelt, G. H. J. van den Oord, M. R. Dobber, A. Malkki, H. Visser, J. de Vries, P. Stammes, J. Lundell, and H. Saari, "The Ozone Monitoring Instrument," *IEEE Trans. Geosci. Remote Sens.*, vol. 44, no. 5, pp. 1093–1101, May 2006.
[19] P. F. Levelt, E. Hilsenrath, G. W. Lippelmeier, G. J. B. van den Oord, P. K. Bhartia, J. Tamminen, J. F. de Haan, and J. P. Veefkind, "Science objectives of the Ozone Monitoring Instrument," *IEEE Trans. Geosci. Remote Sens.*, vol. 44, no. 5, pp. 1199–1208, May 2006.
[20] M. R. Dobber *et al.*, "Ozone Monitoring Instrument calibration," *IEEE Trans. Geosci. Remote Sens.*, vol. 44, no. 5, pp. 1209–1238, May 2006.
[21] G. H. J. van den Oord, "OMI level 0 to 1b processing and operational aspects," *IEEE Trans. Geosci. Remote Sens.*, vol. 44, no. 5, pp. 1380–1397, May 2006.

[22] P. K. Bhartia and C. W. Wellemeyer, "TOMS-V8 total ozone algorithm," in *OMI Algorithm Theoretical Basis Document, OMI Ozone Products*, P. K. Bhartia, Ed. Greenbelt, MD: NASA/Goddard Space Flight Center, 2002, vol. 2.
[23] C. Wellemeyer, P. K. Bhartia, S. L. Taylor, W. Qin, and C. Ahn, "Version 8 Total Ozone Mapping Spectrometer (TOMS) algorithm," in *Proc. Quadrennial Ozone Symp.*, Greece, 2004, pp. 635–636.
[24] A. J. Krueger, N. Krotkov, S. Datta, O. Dubovik, and D. Flittner, "OMI SO_2 algorithm, in OMI ATBD," in *Trace Gas Algorithms*, K. Chance, Ed. Greenbelt, MD: NASA/Goddard Space Flight Center, 2002, vol. 4.
[25] T. McGee and J. Burris, "SO_2 absorption cross sections in the near UV," *J. Quant. Spectrosc. Radiat. Transf.*, vol. 37, no. 2, pp. 165–182, 1987.
[26] N. A. Krotkov, A. J. Krueger, and P. K. Bhartia, "Radiative transfer model of volcanic plumes," *J. Geophys. Res*, vol. 102, no. D18, pp. 21 891–21 904, 1997.
[27] (2005) Sulfur dioxide plume from Manam volcano. NASA Earth Observatory. [Online]. Available: http://earthobservatory.nasa.gov/Newsroom/NewImages/images.php3?img_id=16820
[28] (2005) Eruption of Anatahan. NASA Earth Observatory. [Online]. Available: http://earthobservatory.nasa.gov/NaturalHazards/natural_hazards_v2.php3?img_id=12711
[29] (2005) Sulfur dioxide leaks from Ambrym Volcano. NASA Earth Observatory. [Online]. Available: http://earthobservatory.nasa.gov/NaturalHazards/natural_hazards_v2.php3?img_id=12795
[30] S. A. Carn, N. A. Krotkov, and A. J. Krueger, "Peruvian copper smelter emissions measured by the Ozone Monitoring Instrument," *Geophys. Res. Lett.*, 2006, submitted for publication.
[31] W. G. Read, NASA Jet Propulsion Laboratory, Pasadena, CA, Apr. 14, 2005.
[32] B. Galle, C. Oppenheimer, A. Geyer, A. J. S. McGonigle, M. Edmonds, and L. A. Horrocks, "A miniaturised ultraviolet spectrometer for remote sensing of SO_2 fluxes: A new tool for volcano surveillance," *J. Volcanol. Geotherm. Res.*, vol. 119, pp. 241–254, 2003.
[33] (2005) Network for Observation of Volcanic and Atmospheric Change (NOVAC). [Online]. Available: http://129.16.35.206/

Nickolay A. Krotkov received the B.A. degree in physics and the M.S. degree in remote sensing in 1985 from Moscow Institute of Physics and Technology, Moscow, Russia. He received the Ph.D. degree in oceanography (physics and mathematics) from the P.P. Shirshov Institute of Oceanology, Russian Academy of Sciences, Moscow, Russia, in 1990 for research on using polarization properties of light in oceanic remote sensing.

He joined NASA, Goddard Space Flight Center (GSFC), Greenbelt, MD, in 1993 where he worked on applications of satellite data, such as global mapping of surface ultraviolet (UV) irradiance and generation of UV volcanic eruption data products from the NASA Total Ozone Mapping Spectrometer (TOMS) missions. His main field of research is radiative transfer modeling, satellite– and ground-based UV data analysis and inversions. He is currently a Senior Research Scientist with Goddard Earth Sciences and Technology (GEST) Center, University of Maryland Baltimore County at NASA/GSFC, Greenbelt, Maryland.

Dr. Krotkov is a member of American Geophysical Society.

Simon A. Carn received the B.A. degree in earth science from Oxford University, Oxford, U.K., in 1993 and the DEA degree in volcanology/magmatic processes from Université Blaise Pascal, Clermont-Ferrand, France, in 1994. He received the Ph.D. in volcanology from the Department of Earth Sciences, Cambridge University, Cambridge, U.K., in 1999 for research on volcanism in Indonesia.

From 2000 to 2001, he worked as a volcanologist on the active volcanic island of Montserrat (West Indies). In 2001, he joined the Joint Center for Earth Systems Technology (JCET), University of Maryland Baltimore County (UMBC), Baltimore, to work on remote sensing of volcanic sulfur dioxide (SO_2) emissions using UV satellite data from the NASA Total Ozone Mapping Spectrometer (TOMS) missions and lately from the Ozone Monitoring Instrument (OMI) on the EOS/Aura spacecraft. His main research interests are satellite and ground-based UV/IR data analysis applied to studies of volcanic degassing, eruption monitoring, and air pollution monitoring. He is currently an Assistant Research Scientist with JCET.

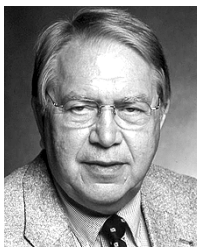

Arlin J. Krueger received the B.A. degree in physics from the University of Minnesota, Minneapolis, in 1955 and the Ph.D. degree in atmospheric sciences from Colorado State University, Fort Collins, in 1984.

He is a Research Professor in the Department of Physics, University of Maryland, Baltimore County. He initially developed rocket instruments to measure atmospheric ozone from 1959 to 1969 at the Naval Weapons Center, China Lake, CA. From 1969 to 2000, he developed satellite instruments and remote sensing techniques at Goddard Space Flight Center, Greenbelt, MD. His primary instrument, the Total Ozone Mapping Spectrometer (TOMS) was noted for the detection of the Antarctic Ozone Hole and for its measurements of volcanic eruption sulfur dioxide clouds. Currently at UMBC, he serves as Principal Investigator for development of SO_2 algorithms for the Aura/ OMI Science Team and for development of near real-time volcanic cloud products for aviation hazard avoidance.

Pawan K. Bhartia received the M.S. degree in computer science and the Ph.D. degree in physics in 1977 from Purdue University, West Lafayette, IN.

He is currently the Project Scientist of NASA's Total Ozone Mapping Spectrometer (TOMS) satellite mission and the U.S. Science Team Leader of the Ozone Monitoring Instrument (OMI) on EOS Aura. He has over 60 scientific publications, dealing principally with the measurement of the Earth's ozone layer.

Dr. Bhartia has received several NASA awards for his work, including the prestigious William Nordberg Medal in Earth Science from NASA Goddard Space Flight Center.

Kai Yang received the B.S.degree from Sun Yat-Sen University, Guangzhou, China, in 1984 and the Ph.D. degree from Kansas State University, Manhattan, in 1991, both in physics.

He joined the Chemistry Department, Princeton University, Princeton, NJ, where he conducted theoretical research on the scattering and absorption of atoms on solid surfaces. In 1993, he joined NASA Goddard Space Flight Center and performed radiative transfer simulations of the Moderate Resolution Imaging Spectroradiometer (MODIS) measurements and developed the MODIS level 2 gridded products. Later, he joined the Ozone Monitoring Instrument (OMI) science support team in 2001, working on advanced algorithms for total ozone retrieval. His research interests include spectral fitting and optimal estimation methods for trace gas retrieval, atmospheric radiative transfer modeling, rotational Raman scattering, and remote sensing data analysis and applications. He is currently a Senior Scientist with Science Systems and Applications, Inc., Lanham, MD.